Point Interpolation Methods for phase-field modelling of brittle fracture

Larissa Novelli[1], Lapo Gori[1], Roque L. S. Pitangueira[1]

[1]*Dept. of Structural Engineering, Federal University of Minas Gerais*
Pres. Antonio Carlos, 6627, School of Engeneering - Bulding 1, Pampulha, Belo Horizonte/MG, Brazil
larissan@ufmg.br, lapo@dees.ufmg.br, roque@dees.ufmg.br

Abstract. The present work investigates the application of meshfree Point Interpolation Methods (PIM) to the phase-field modelling of brittle fracture. The phase-field modelling is an efficient tool for the simulation of complex cracks. Within this approach, a crack is modelled as a diffuse crack where a length scale parameter controls the size of diffusive region and the value of phase-field indicates the integrity of the material. Point Interpolation Methods can be based on polynomial or radial shape functions. These shape functions possess (i) the Kronecker delta property, that allows a more simple imposition of essential boundary conditions, (ii) the compact support property and (iii) the partition of unity property. This paper discusses the computational aspects of the application of the PIM strategy to the phase-field modelling, and presents numerical simulations to illustrate the characteristics of the proposed approach.

Keywords: Meshfree methods, Point Interpolation Methods, Phase-field modelling, Brittle fracture

1 Introduction

The phase-field is an important method for the modelling of complex cracks. This approach was proposed by Francfort and Marigo [1] as the reformulation of a potential energy minimization problem based on Griffith's theory [2]. The crack is modelled as a diffuse entity and the crack initiation, propagation and branching are obtained directly from the solution of the crack phase-field and mechanical equilibrium equations. Anisotropic models, which divide the energy associated to traction and compressive regions, were proposed to prevent cracks in compressive regions of the model [3].

In recent works, the combination of meshfree mesthods and phase-field modelling has been proposed [4–6]. In these methods, the nodes are not connected through elements and have the advantage of not needing to implement conforming meshes and not presenting the issue of distortion of elements. The approximation functions are built using a set of nodes in the neighbourhood of the point, called support nodes.

This paper investigates the use of the meshfree Point Interpolation Method (PIM) for the analysis of quasi-brittle problems with the phase-field approach. The polynomial and radial shape functions are investigated in two numerical examples. The simulations are performed using the INSANE (Interactive Structural ANalisys Environment) [1].

2 Phase-field modelling of brittle fracture

In the phase-field modelling, the crack present in a domain Ω is modelled as a diffuse entity, as shown in Fig. 1. A length scale parameter l_0 defines the width of the diffuse region and the scalar value of the phase-field indicate the state of the material, being 0 for intact material and 1 for completely broken material.

The diffuse crack is represented in terms of a crack surface density function, expressed by:

$$\gamma(\phi, \nabla\phi) = \frac{1}{2l_0}\phi^2 + \frac{l_0}{2}|\nabla\phi|^2 \tag{1}$$

---

[1]More information on the project can be found at https://www.insane.dees.ufmg.br/; the development code is freely available at the Git repository http://git.insane.dees.ufmg.br/insane/insane.git.
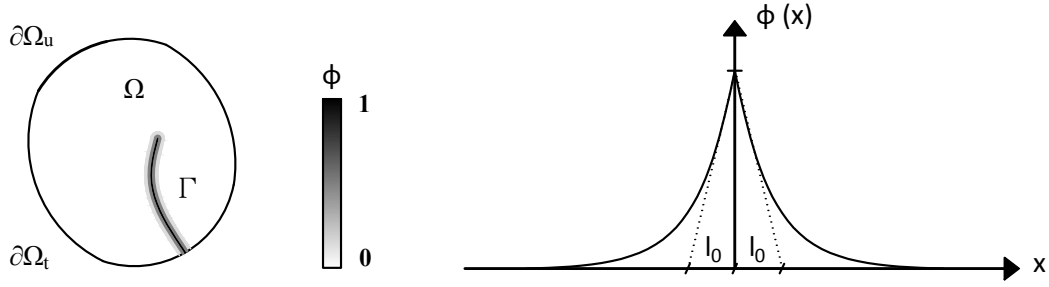
Figure 1. Phase-field modelling for diffuse crack.

The total energy functional of the body is given by:

$$E_t = \int_\Omega \psi(\boldsymbol{\varepsilon}(\boldsymbol{u}), \phi) dV + \int_\Omega G_c \gamma(\phi, \nabla\phi) dV - \int_\Omega \boldsymbol{b} \cdot \boldsymbol{u} dV - \int_{\partial\Omega} \boldsymbol{t} \cdot \boldsymbol{u} dA \tag{2}$$

where G_c is the fracture energy, $\boldsymbol{b}$ is the body forces and $\boldsymbol{t}$ is the surface forces.

The term $\psi(\boldsymbol{\varepsilon}(\boldsymbol{u}), \phi)$ is the elastic strain energy density, that is related to the phase-field through the function $g(\phi)$ called degradation function, that in this paper is given by:

$$g(\phi) = (1 - \phi)^2 + k \tag{3}$$

where k is a small value used to prevent numerical singularities. In the isotropic model [7], the function $g(\phi)$ is applied in all domain as the Eq. 4:

$$\psi(\boldsymbol{\varepsilon}(\boldsymbol{u}), \phi) = g(\phi)\psi_0(\varepsilon) \tag{4}$$

In the anisotropic models, to prevent cracks growth under compression, the function $g(\phi)$ is applied to the positive part of the strain energy ($\psi_0^+(\varepsilon)$) as

$$\psi(\boldsymbol{\varepsilon}(\boldsymbol{u}), \phi) = g(\phi)\psi_0^+(\varepsilon) + \psi_0^-(\varepsilon) \tag{5}$$

Different authors proposed the decomposition of the strain energy. In this paper, the spectral decomposition of the strain tensor discussed by Miehe et al. [3] is used.

The governing equations of the phase-field problem in the weak form are:

$$\begin{cases} \int_\Omega \boldsymbol{\sigma} : \delta\boldsymbol{\varepsilon} dV = \delta P_{ext} \\ \int_\Omega [2(1-\phi)H\delta\phi + \frac{G_c}{l_0}\phi\delta\phi + G_c l_0 \nabla\phi \cdot \nabla\delta\phi] dV \geq 0 \end{cases} \tag{6}$$

where the term H is the historical variable discussed by Miehe et al. [3] and it is defined as the maximum strain energy in the traction region.

3 Point Interpolation Methods

The PIM obtains its approximation by letting the interpolation function pass through the function values at each scattered node within the support domain [8]. This method was proposed by Liu and Gu [9], where polynomial functions were used. To guarantees the existence of the inverse of the moment matrix present in the formulation, Wang and Liu [10] suggested the use of radial basis functions, originating the Radial Point Interpolation Method (RPIM). The RPIM with pure radial functions is not (polynomial) consistent and has a problem passing the standard patch tests, meaning that it fails to reconstruct the linear (polynomial) field exactly [8]. Wang and Liu [11] proposed adding polynomial basis functions to restore the consistency of RPIM shape functions, resulting radial point interpolation method with polynomial reproduction (RPIMp).

All these shape functions possess the Kronecker delta function property, which allows for an easy treatment of essential boundary conditions. Besides this property, they have the partition of unity and the compact support domain, and don't rely on weight functions as in the Moving Least Square approach.

The PIM shape function for a node k at a point $\mathbf{x}$ is given by:

$$N_k(\mathbf{x}) = \sum_{i=1}^n P_i(\mathbf{x})(P_m^{-1})_{ik}. \tag{7}$$

where n is the number of nodes in the neighbourhood of $\mathbf{x}$, P_i are the polynomial basis functions and $\mathbf{P}_m$ is the moment matrix.

$$\mathbf{P}_m^T = [\mathbf{p}(\mathbf{x}_1), \mathbf{p}(\mathbf{x}_2), \mathbf{p}(\mathbf{x}_3), ..., \mathbf{p}(\mathbf{x}_n)] \tag{8}$$

In this shape function, 3 or 6 polynomial terms are used, depending on the number of support nodes.

The RPIMp shape function for a node k at a point $\mathbf{x}$ is given by:

$$N_k(\mathbf{x}) = \sum_{i=1}^{n} R_i(\mathbf{x})S_{ik}^a + \sum_{j=1}^{m} P_j(\mathbf{x})S_{jk}^b. \tag{9}$$

where n is number of nodes in the neighbourhood of $\mathbf{x}$, m is a number of monomials composing the polynomial basis, R_i are the radial basis functions, P_j are the polynomial basis functions, and the matrix $\mathbf{S}_a$ and $\mathbf{S}_b$ are:

$$\mathbf{S}_a = \mathbf{R}_Q^{-1}[1 - \mathbf{P}_m\mathbf{S}_b] = \mathbf{R}_Q^{-1} - \mathbf{R}_Q^{-1}\mathbf{P}_m\mathbf{S}_b. \tag{10}$$

$$\mathbf{S}_b = [\mathbf{P}_m^T\mathbf{R}_Q^{-1}\mathbf{P}_m]^{-1}\mathbf{P}_m^T\mathbf{R}_Q^{-1} \tag{11}$$

where $\mathbf{R}_Q$ is the moment matrix of the radial function and $\mathbf{P}_m$ is the moment matrix of the polynomial function. In this paper, the following exponential radial function with the scaled distance $R_i(r_i^*)$ and polynomial functions with 3 polynomial terms are adopted.

$$R_i(r_i^*) = \exp(-cr_i^{*2}) \tag{12}$$

where r_i^* is the scaled distance and c is a shape parameter which controls the decay rate of the function. The scaled distance is adopted in order to obtain a function less dependent on the nodal spacing

$$r_i^* = \frac{r_i}{max(r)} \qquad r_i = \sqrt{(x - x_i)^2 + (y - y_i)^2} \tag{13}$$

where r_i is the distance between the point $\mathbf{x}$ and the i-th support node and $max(r)$ is the maximum r_i found in the support domain.

The construction of the shape functions at each point of interest $\mathbf{x}$ require the use of a number of support nodes in the neighbourhood of that point. This support nodes can be obtained using the T-schemes for nodes selection. T-schemes are based in cells of triangular type, as shown in the Fig. 2. In this work, T3 and T6/3 schemes are used.

(a) T3-scheme   (b) T6/3-scheme
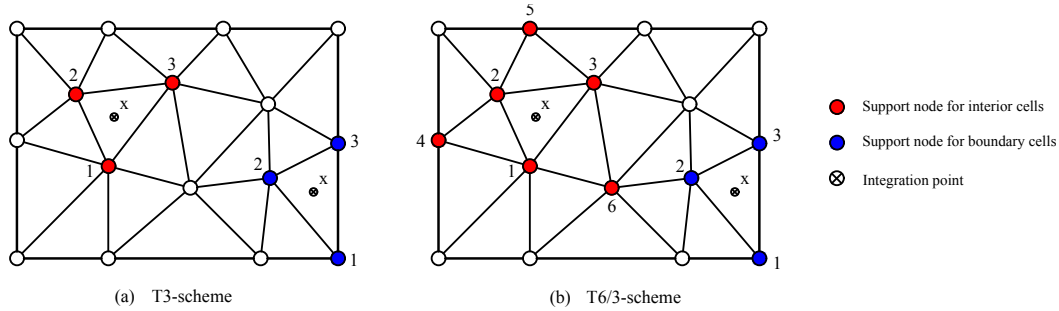
Figure 2. T-schemes for nodes selection.

4 PIM discretisation of the phase-field model

The displacement field $\boldsymbol{u}$ and phase-field ϕ are approximated using PIM shape functions as

$$\boldsymbol{u}(\mathbf{x}) = \sum_{I=1}^{SN} \boldsymbol{N}_I(\mathbf{x})\boldsymbol{d}_I \qquad \phi(\mathbf{x}) = \sum_{I=1}^{SN} N_I(\mathbf{x})a_I \tag{14}$$

where SN are the support nodes, $\boldsymbol{d}_I$ and a_I are the nodal values of the displacements and phase-field, respectively. The strain tensor and gradient of the phase-field are given by

$$\varepsilon(\mathbf{x}) = \sum_{I=1}^{SN} \boldsymbol{B}_I^u(\mathbf{x}) \boldsymbol{d}_I \qquad \nabla\phi(\mathbf{x}) = \sum_{I=1}^{SN} \boldsymbol{B}_I^\phi(\mathbf{x}) a_I \tag{15}$$

where

$$\boldsymbol{B}_I^u(\mathbf{x}) = \begin{bmatrix} N_{I,x}^u & 0 \\ 0 & N_{I,y}^u \\ N_{I,y}^u & N_{I,x}^u \end{bmatrix} \qquad \boldsymbol{B}_I^\phi(\mathbf{x}) = \begin{bmatrix} N_{I,x}^\phi \\ N_{I,y}^\phi \end{bmatrix} \tag{16}$$

where $N_{I,x}$ and $N_{I,y}$ are the derivatives of the shape functions.

Replacing the expressions above in to Eq. 6 results in the following:

$$\int_\Omega (\boldsymbol{B}^u)^T \boldsymbol{\sigma}\, dV = f_{ext} \tag{17}$$

$$\int_\Omega 2(1-\phi)H(\boldsymbol{N}^\phi)^T dV + \int_\Omega (\frac{G_c}{l_0}\phi(\boldsymbol{N}^\phi)^T + G_c l_0 (\boldsymbol{B}^\phi)^T \nabla\phi) dV \geq 0. \tag{18}$$

For the numerical integration, one integration point is considered in the center of each cell and the staggered solution scheme [12] is used to solve the Eq. 17 and 18.

5   Numerical simulations

This section illustrates the numerical results obtained by PIM to the modelling of the phase-field of brittle fracture. Two examples present in the literature are analysed. For each problem, PIM and RPIM shape functions were adopted, as well as T3 and T6/3 schemes for nodes selection. For comparison purposes, the results obtained with the FEM were presented, performed using the same triangular meshes of the cells.

5.1   Shear test

This example is characterised by a crack evolution only in the traction region of the problem. The shear test illustrated in Fig. 3(a) was simulated by Miehe et al. [3], using an anisotropic model; the same model has been adopted here in combination with the PIM approach. The material was modelled considering a Young's modulus $E = 210$ kN/mm^2, Poisson's ratio $\nu = 0.3$, critical energy release rate $G_c = 0.0027$ kN/mm and length scale parameter $l_0 = 0.015$ mm. The nodal distribution, FEM mesh and background mesh are shown in Figs. 3(b) and 3(c).
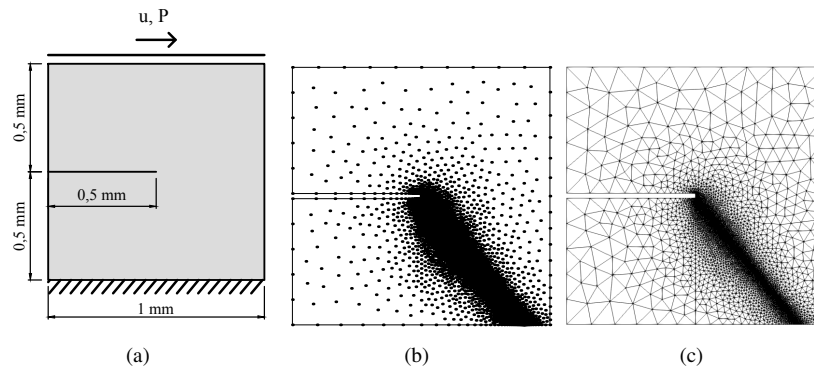
Figure 3. Shear test: (a) Geometry, loading and boundary conditions, (b) Nodal distribution, and (c) FEM mesh and background mesh.

The nonlinear process was performed by the direct displacement control method, considering increments of $\Delta u = 1 \times 10^{-4}$ mm of the top edge in the horizontal direction for all the steps. The load-displacement curves are shown in Fig. 4 together with the reference solution by Miehe et al. [3]. For all the strategies, the peak load factor was greater than the one of the reference. In the authors opinion, this behaviour is most probably due to the

differences between the current and reference meshes, since the phase-field approach is quite sensitive to the mesh density as observed in Patil et al. [13]. For the T3 scheme, the curves obtained with FEM, PIM and RPIMp are the same. For the T6/3 scheme, the strategies fail to complete the analysis.

(a) T3 scheme   (b) T6/3 scheme

——— Miehe et al. [2]   ●— FEM   ●— PIM   ●— RPIMp
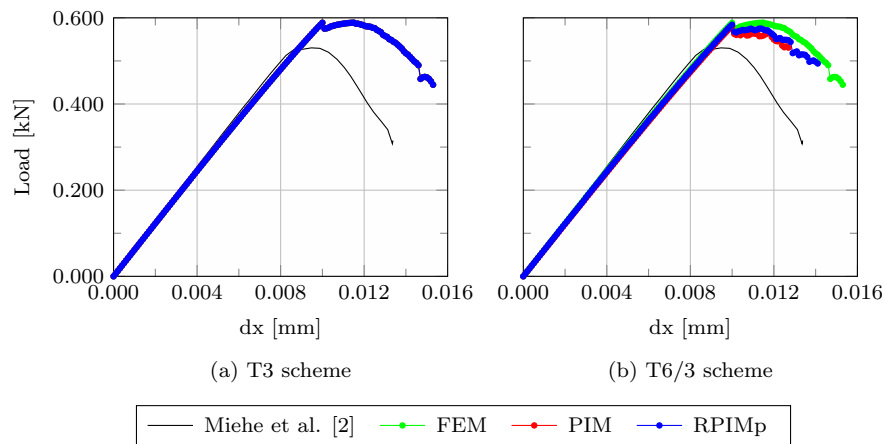
Figure 4. Load-displacement curve of the shear test.

The contour plots of the nodal values of the phase-field for the RPIM-T3 are illustraded in Fig. 5. It is possible observe that this strategy is able to indicate the nucleation and propagation of the cracks presented in Miehe et al. [3].

(a)   (b)   (c)
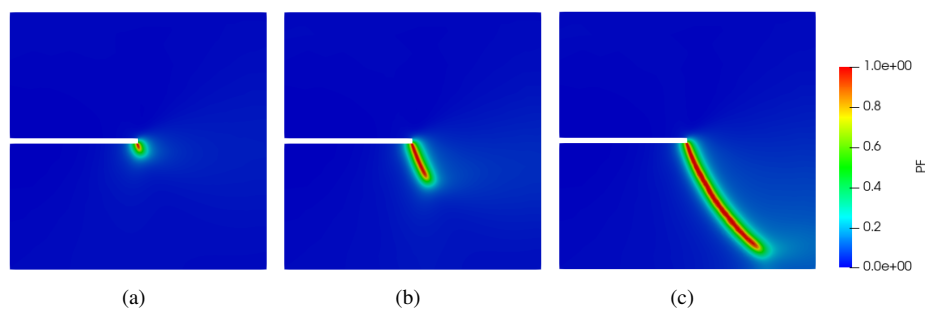
Figure 5. Phase-field contour plots for the shear test with PIM-T3. Displacements of (a) 1.01×10^{-2} mm, (b) 1.20×10^{-2} mm and (c) 1.53×10^{-2} mm.

5.2 Bi-material tensile test

This example shows the ability to model the crack branching phenomenon. The bi-material tensile test illustrated in Fig. 6(a) was simulated by Molnar and Gravouil [14]. The "Material 1" indicated in Fig. 6(a) is characterised by a Young's modulus E = 377 kN/mm^2, Poisson's ratio $\nu = 0.3$, critical energy release rate G_c = 0.01 kN/mm and length scale parameter $l_0 = 0.3$ mm, while the "Material 2" is characterised by a Young's modulus E = 37.7 kN/mm^2, Poisson's ratio $\nu = 0.3$, critical energy release rate G_c = 0.001 kN/mm and length scale parameter $l_0 = 0.3$ mm. Similar to the Molnar and Gravouil [14], the isotropic model is adopted. The nodal distribution, FEM mesh and background mesh to T-schemes are shown in Figs. 6(b) and 6(c).

The nonlinear process was performed by the direct displacement control method, considering increments of $\Delta u = 2 \times 10^{-4}$ mm of the right edge in the horizontal direction for all the steps. The load-displacement curves are shown in Fig. 7 together with the reference solution obtained by Molnar and Gravouil [14]. The curves obtained for all strategies are similar to the reference curves, except for the different displacement values corresponding to the first fracture progation between Figs. 8(a) and 8(b), and the last propagation illustrated in Fig. 9.

The contour plots of phase-field for the PIM-T3 are illustraded in Fig. 8. It is possible observe that crack propagates in the direction of the initial crack in the lower material up to the the transition zone. Then, the crack branching occurs and two cracks propagate along the interface. As pointed out by Molnar and Gravouil [14] the branching occurs because the energy required for the branch is less than the energy required to propagate through the tougher material. Fig. 9 presents the final step of the analysis, where the crack propagates through the tougher

material and the force is abruptly reduced. These results are similar to those presented in Molnar and Gravouil [14].

| (a) | (b) | (c) |
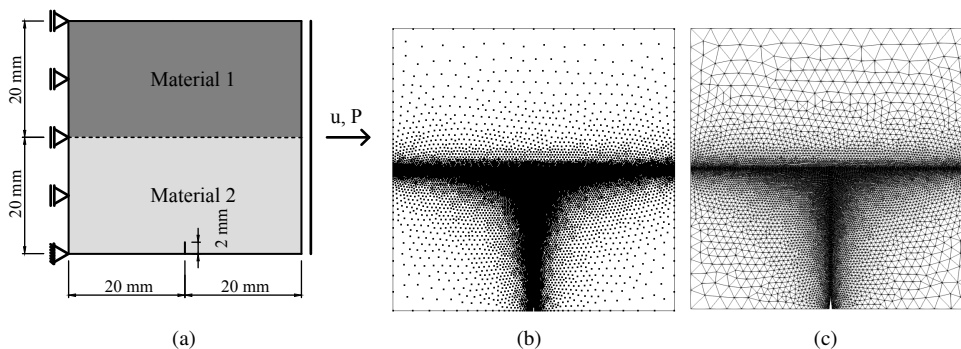
Figure 6. Bi-material tensile test: (a) Geometry, loading and boundary conditions, (b) Nodal distribution, and (c) FEM mesh and background mesh.

(a) T3 scheme   (b) T6/3 scheme

Molnar ——   FEM ●——   PIM ●——   RPIMp ●——
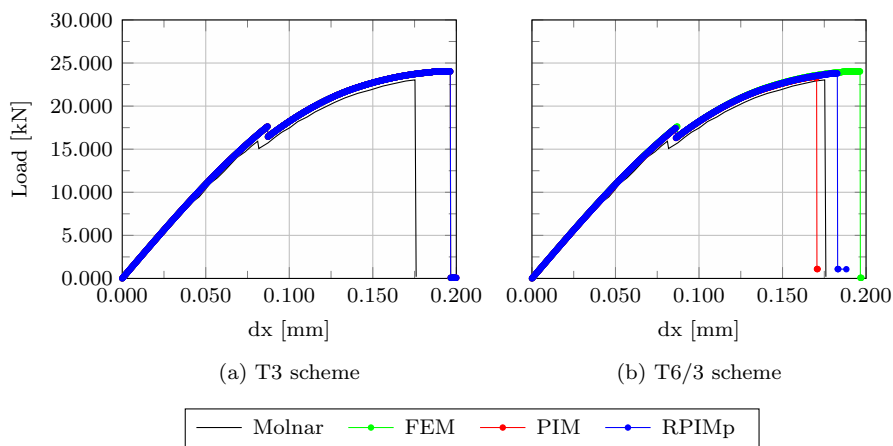
Figure 7. Load-displacement curve of the bi-material tensile test.

6 Conclusions

This paper presented the application of the PIM meshfree method for discretisation of the phase-field modelling for fracture. PIM and RPIMp shape functions were used with T3 and T6/3 schemes for support nodes selection. Two numerical simulations were presented comparing the proposed strategies with FEM and the reference solution. In the two examples performed, the load-displacement curves that were obtained presented a good agreement with the results of the literature and the results obtained with T3 schemes were the same as the ones obtained with the FEM. In the case of the shear test example, the strategies with T6/3 schemes presented curves with instablities. It is possible to observe that in both simulations, the contour plots for the phase-field are similar to those of the literature. The use of the PIM meshfree method with phase-field modelling was able to simulate crack nucleation, propagation and branching.

Authorship statement. The authors hereby confirm that they are the sole liable persons responsible for the authorship of this work, and that all material that has been herein included as part of the present paper is either the property (and authorship) of the authors, or has the permission of the owners to be included here.
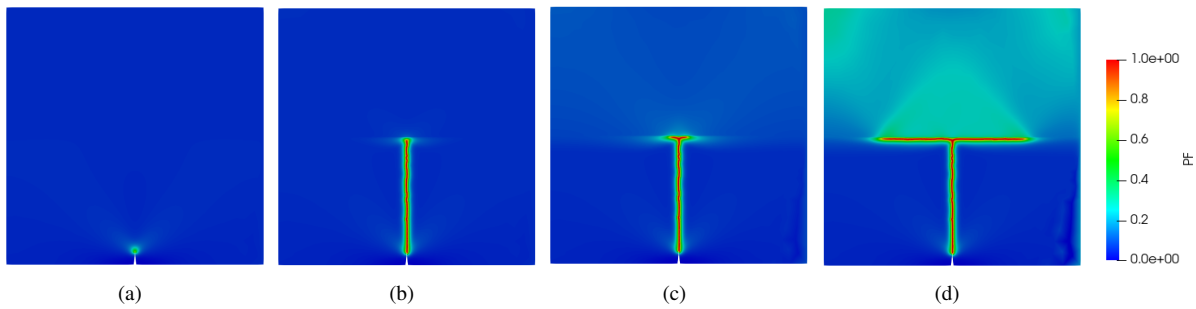
Figure 8. Phase-field contour plots for the bi-material tensile test with RPIMp-T3. Displacements of (a) 0.086 mm, (b) 0.0872 mm, (c) 0.12 mm and (c) 0.194 mm.
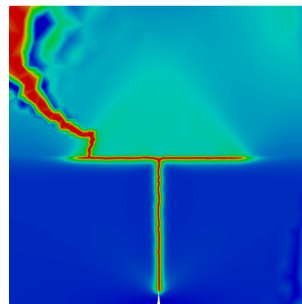
Figure 9. Final fracture of the bi-material tensile test.

References

[1] G. A. Francfort and J. J. Marigo. Revisiting brittle fracture as an energy minimization problem. *J Mech Phys Solids*, vol. 46, 1998.

[2] A. A. Griffith. The phenomena of rupture and flow in solids. *Philos Trans R Soc Lond Ser*, vol. 221, pp. 163–198, 1921.

[3] C. Miehe, F. Welschinger, and M. Hofacker. Thermodynamically consistent phase-field models of fracture: Variational principles and multi-field fe implementations. *International Journal for Numerical Methods in Engineering*, vol. 83, pp. 1273–1311, 2010.

[4] J. Wu, D. Wang, Z. Lin, and D. Qi. An efficiente gradient smoothing meshfree formulation for the fourth-order phase field modeling of brittle fracture. *Computation Particle Mechanics*, vol. 7, pp. 193–207, 2019.

[5] Y. Shao, Q. Duan, and S. Qiu. Adaptive consistent element-free galerkin method for phase-field model of brittle fracture. *Computational Mechanics*, vol. 64, pp. 741–767, 2019.

[6] P. Kasirajan, S. Bhattacharya, M. Arroyo, A. Rajagopal, and J. N. Reddy. Phase field modeling of fracture in quasi-brittle materials using natural neighbor galerkin method. *Computer methods in applie mechanics and engineering*, vol. 366, pp. 113019, 2020.

[7] B. Bourdin, G. A. Francfort, and J. J. Marigo. Numerical experiments in revisited brittle fracture. *J Mech Phys Solids*, vol. 48, 2000.

[8] G. R. Liu. *Meshfree Methods: Moving Beyond the Finite Element method*. CRC Press, New York, 2009.

[9] G. R. Liu and Y. T. Gu. A point interpolation method for two-dimensional solids. *International Journal for Numerical Methods in Engineering*, vol. 50, pp. 937–951, 2001.

[10] J. G. Wang and G. R. Liu. A radial point interpolation method for elastoplastic problems. In *Fist International Conference on Structural Stability and Dynamics*, pp. 703–708, Taipei, Taiwan, 2000.

[11] J. G. Wang and G. R. Liu. A point interpolation meshless method based on radial basis functions. *International Journal for Numerical Methods in Engineering*, vol. 54, pp. 1623–1648, 2002.

[12] F. Zhang, W. Huang, X. Li, and S. Zhang. Moving mesh finite element simulation for phase field of fracture and convergence of newton's iteration. *Journal of Computational Physics*, vol. 356, pp. 127–149, 2018.

[13] R. U. Patil, B. K. Mishra, and I. V. Singh. An adaptive multiscale phase field method for brittle fracture. *Computer Methods in Applied Mechanics and Engineering*, vol. 329, pp. 254–288, 2017.

[14] G. Molnar and A. Gravouil. 2d and 3d abaqus implementation of a robust staggered phase-field solution for modeling brittle fracture. *Finite Elements in Analysis and Design*, vol. 130, pp. 27–38, 2017.